Repo-Man recruits PP1γ to chromatin and is essential for cell viability

Laura Trinkle-Mulcahy,[1] Jens Andersen,[2] Yun Wah Lam,[1] Greg Moorhead,[3] Matthias Mann,[2] and Angus I. Lamond[1]

[1]University of Dundee, Dundee DD1 5EH, Scotland, UK
[2]University of Southern Denmark, Odense Campusvej 55, DS-5230 Odense M, Denmark
[3]University of Calgary, Calgary, Alberta, Canada T2N 1N4

Protein phosphatase 1 (PP1) is a ubiquitous serine/threonine phosphatase regulating many cellular processes. PP1α and -γ are closely related isoforms with distinct localization patterns, shown here by time-lapse microscopy of stably expressed fluorescent protein fusions. A pool of PP1γ is selectively loaded onto chromatin at anaphase. Using stable isotope labeling and proteomics, we identified a novel PP1 binding protein, Repo-Man, which selectively recruits PP1γ onto mitotic chromatin at anaphase and into the following interphase. This approach revealed both novel and known PP1 binding proteins, quantitating their relative distribution between PP1α and -γ in vivo. When overexpressed, Repo-Man can also recruit PP1α to chromatin. Mutating Repo-Man's PP1 binding domain does not disrupt chromatin binding but abolishes recruitment of PP1 onto chromatin. RNA interference–induced knockdown of Repo-Man caused large-scale cell death by apoptosis, as did overexpression of this dominant-negative mutant. The data indicate that Repo-Man forms an essential complex with PP1γ and is required for the recruitment of PP1 to chromatin.

Introduction

Reversible protein phosphorylation is the major general mechanism regulating most physiological processes in eukaryotic cells. Hundreds of protein kinases have been identified to date, with significantly fewer phosphatases found to counteract their action. This discrepancy can be explained in part by mechanisms used to control phosphatase activity. Protein phosphatase 1 (PP1), a major serine/threonine protein phosphatase involved in a wide range of cellular processes, exists in the cell as an oligomeric complex. The core catalytic subunit binds a spectrum of interacting proteins, termed targeting subunits, that modulate both its intracellular localization and substrate specificity (for review see Cohen, 2002). Most of the known targeting subunits, including those targeting PP1 to such substrates as glycogen and myosin, contain a conserved "RVXF" motif (consensus Arg/Lys-Val/Ile-Xaa-Phe/Trp; Egloff et al., 1997) that mediates direct binding to PP1. Using primarily biochemical approaches, >50 PP1 targeting subunits have been identified. However, these most likely cannot account for the large number of regulatory pathways in which PP1 plays a critical role, suggesting that many targeting subunits remain to be discovered.

In addition to the signaling diversity provided by targeting subunits, PP1 is also expressed in mammalian cells as three closely related isoforms, α, β/δ, and γ, which are encoded by separate genes. These isoforms are >89% identical in amino acid sequence, with minor differences primarily at their NH_2 and COOH termini (for review see Cohen, 2002). Although most biochemical studies have not directly addressed the significance of the different isoforms, in vivo data show that they have distinct subcellular localization patterns (Andreassen et al., 1998; Trinkle-Mulcahy et al., 2001). This implies differences in their specificity of interaction with particular targeting proteins and hence preferential incorporation into different signaling complexes.

Expression of PP1 isoforms as fusions with fluorescent protein (FP) tags offers both a means to compare their targeting in living cells and a method to recover them from cell lysates and analyze the proteins with which they associate. Because of the unreliability of commercially available PP1 isoform–specific antibodies for immunostaining (Trinkle-Mulcahy et al., 2003; Lesage et al., 2004), we have gone to great lengths to validate the use of these FP fusion proteins as markers for endogenous pools of PP1. FP-tagged PP1 isoforms are functionally active phosphatases with distinct interphase localization

Correspondence to Laura Trinkle-Mulcahy: l.trinklemulcahy@dundee.ac.uk

Abbreviations used in this paper: DIC, differential interference contrast; FP, fluorescent protein; FRET, fluorescent resonance energy transfer; PP1, protein phosphatase 1; RNAi, RNA interference; siRNA, small interfering RNA; SILAC, stable isotope labeling of amino acids in cell culture.

The online version of this article contains supplemental material.

The Journal of Cell Biology, Vol. 172, No. 5, February 27, 2006 679–692
http://www.jcb.org/cgi/doi/10.1083/jcb.200508154

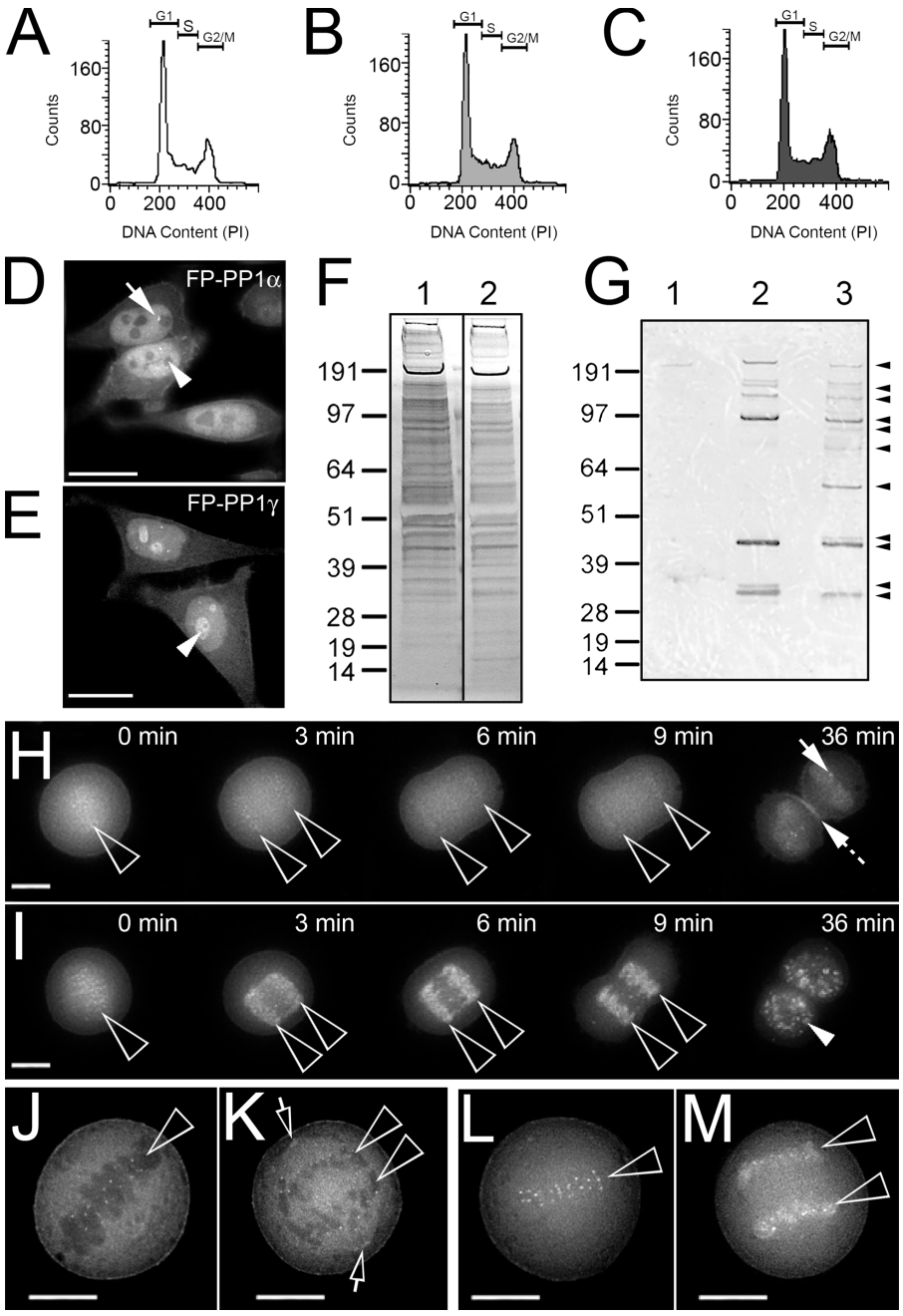

Figure 1. **Intrinsic differences between FP-PP1α and FP-PP1γ expressed stably in mammalian cells.** (A–C) FACS analyses show no significant difference in cell cycle distribution between HeLa$^{EGFP\text{-}PP1\alpha}$ (B) and HeLa$^{EGFP\text{-}PP1\gamma}$ (C) cells and parental HeLa cells (A). (D and E) Fluorescence imaging of the stable cell lines during interphase reveals distinct localization patterns for FP-PP1α (D) and FP-PP1γ (E), with nucleoli (arrowheads) and FP-PP1α foci (arrow) marked. (F) FP-PP1α (lane 1) and FP-PP1γ (lane 2) immunoprecipitates separated by one-dimensional SDS-PAGE and silver stained. (G) Far Western overlay with ^{35}S-PP1 shows differences (arrowheads) between FP-PP1α (lane 2) and FP-PP1γ (lane 3) immunoprecipitates. FP alone (lane 1) does not coprecipitate PP1 binding proteins. (H and I) Time-lapse imaging of HeLa$^{EGFP\text{-}PP1\alpha}$ (H) and HeLa$^{EGFP\text{-}PP1\gamma}$ (I) cells during mitosis shows differences in localization with respect to chromatin (open arrowheads). Although both accumulate at kinetochores in metaphase (0 min), FP-PP1α is excluded from other chromatin regions, reaccumulating within the nucleus and nuclear foci (solid arrow) in late telophase (36 min), with additional accumulations at the midbody and cell cortex (dotted arrow). In contrast, a large pool of FP-PP1γ appears on chromatin at anaphase (3 min) and remains there, with a pool reentering nucleoli in late telophase (closed arrowhead). (J–M) High-resolution imaging of live mitotic HeLa$^{EGFP\text{-}PP1\alpha}$ cells shows the kinetochore localization and chromatin (arrowheads) exclusion of FP-PP1α during metaphase (J) and anaphase (K), as compared with FP-PP1γ's kinetochore localization at metaphase (L) and sudden chromatin association at anaphase (M). A pool of FP-PP1α is also found on centrosomes (arrows). Bars, 10 μm.

patterns (Trinkle-Mulcahy et al., 2001) matching those observed by antibody staining of endogenous PP1 isoforms in fixed cells (Andreassen et al., 1998). Importantly, these distinct localization patterns can be overridden if a single targeting subunit is exogenously overexpressed in cells (Trinkle-Mulcahy et al., 2001). In this case, the abundantly expressed targeting subunit recruits all PP1 isoforms into the same distribution pattern, suggesting that the expression levels of individual targeting subunits are critical for determining the normal localization patterns of PP1 isoforms.

We recently reported the establishment and characterization of HeLa cell lines stably expressing FP-PP1γ (Trinkle-Mulcahy et al., 2003). During interphase, FP-PP1γ was found in both cytoplasmic and nucleoplasmic pools, showing a prominent accumulation within nucleoli, whereas time-lapse imaging revealed dynamic targeting to specific sites during cell division, including kinetochores and chromatin. This changing spatiotemporal pattern implicates PP1γ in multiple regulatory pathways, in agreement with previous work linking its activity to the regulation of such cellular events as transcription, chromatin remodeling, chromosome condensation and segregation, cytokinesis, and reassembly of the nuclear envelope (for review see Ceulemans and Bollen, 2004).

We have now established a HeLa cell line stably expressing FP-PP1α. The separate HeLa$^{EGFP\text{-}PP1\alpha}$ and HeLa$^{EGFP\text{-}PP1\gamma}$ cell lines allow the contrasting localization patterns and dynamic properties of both isoforms to be analyzed throughout the cell cycle and facilitate a comparison of isoform-specific binding

partners detected via affinity purification of the respective tagged proteins. Mass spectrometry–based proteomics has become a powerful tool for identifying and quantifying the components of multiprotein complexes (for review see de Hoog and Mann, 2004). More recently, several techniques have exploited the use of heavy isotope tags to compare and quantitate relative protein levels under different biological conditions (for review see Ong and Mann, 2005). In the case of stable isotope labeling of amino acids in cell culture (SILAC), cells are metabolically labeled through growth in medium containing a specific amino acid with either carbon or nitrogen or both substituted with the heavy isotopes ^{13}C and ^{15}N. By using substituted arginine or lysine, proteins are labeled specifically at sites of trypsin cleavage, which is convenient for subsequent analysis of tryptic peptides by mass spectrometry.

We adapted the triple encoding SILAC approach (Blagoev et al., 2004) to identify both novel and known PP1-interacting proteins and quantify their relative distribution between PP1α and -γ in vivo. One of these proteins, Repo-Man, defines a novel pool of PP1, selectively involving the γ isoform, which loads onto chromatin at anaphase and remains bound throughout the following interphase. Several lines of evidence indicate that the Repo-Man–PP1 complex is critical for cell viability.

Results

Comparison of HeLa$^{EGFP\text{-}PP1\alpha}$ and HeLa$^{EGFP\text{-}PP1\gamma}$ stable cell lines

A stable HeLa cell line (HeLa$^{EGFP\text{-}PP1\alpha}$) was established that expresses PP1α fused at its NH_2 terminus to EGFP. As observed for the previously characterized HeLa$^{EGFP\text{-}PP1\gamma}$ stable cell line (Trinkle-Mulcahy et al., 2003), this HeLa$^{EGFP\text{-}PP1\alpha}$ cell line is homogenous, with >95% of the cells expressing full-length catalytically active FP-PP1α at levels similar to those of endogenous PP1α (unpublished data). A comparison of the cell cycle progression of both HeLa$^{EGFP\text{-}PP1\alpha}$ and HeLa$^{EGFP\text{-}PP1\gamma}$ cells with parental HeLa cells showed that their growth rates are equivalent, and FACS analysis confirmed that the relative populations in G1, S, and G2/M are similar (Fig. 1, A–C).

Fluorescence imaging of HeLa$^{EGFP\text{-}PP1\alpha}$ and HeLa$^{EGFP\text{-}PP1\gamma}$ cells revealed striking differences in the intrinsic localization patterns of the two isoforms (Fig. 1, D and E), similar to those observed previously by transient transfection of the fusion proteins (Trinkle-Mulcahy et al., 2001) and by antibody labeling of the endogenous proteins (Andreassen et al., 1998). Although both are found in the cytoplasm and in the nucleus throughout G1, S, and G2, nuclear FP-PP1α is found mainly in a diffuse pool and in a few as-yet-unidentified foci (Fig. 1 D, arrow) and largely excluded from nucleoli. In contrast, nuclear FP-PP1γ shows a strong accumulation within nucleoli (Fig. 1 E, arrowhead; ∼20% of the total nuclear FP-PP1γ; Trinkle-Mulcahy et al., 2003).

FP-PP1α and FP-PP1γ also show differences in their dynamic distribution during cell division. Time-lapse imaging revealed that although both isoforms accumulate at kinetochores in metaphase (Fig. 1, H and I, 0 min), FP-PP1α is predominantly excluded from other chromatin regions throughout mitosis (open arrowheads). In contrast, low levels of FP-PP1γ appear on chromatin at metaphase and there is a sudden and rapid recruitment of a larger pool (∼20% of the total cellular pool; Trinkle-Mulcahy et al., 2003) onto chromatin as the cell enters anaphase (Fig. 1 I, 3 min; Trinkle-Mulcahy et al., 2003). Both isoforms also localize at the cortex and midbody in telophase (Fig. 1 H, dotted arrow; Trinkle-Mulcahy et al., 2003). FP-PP1α is recruited back into the nucleus much later in telophase (Fig. 1 H, 36 min), whereas FP-PP1γ, which is already associated with chromatin, reaccumulates within nucleoli at this time (Fig. 1 I, 36 min). High-resolution images of mitotic HeLa$^{EGFP\text{-}PP1\alpha}$ cells more clearly demonstrate the chromatin exclusion of FP-PP1α during metaphase and anaphase (Fig. 1, J and K, arrowheads), as compared with FP-PP1γ and its dramatic recruitment to chromatin at anaphase (Fig. 1, L and M, arrowheads). FP-PP1α also accumulates at centrosomes (Fig. 1 K, arrows), which was confirmed in both interphase and mitotic cells by counterstaining with anti-tubulin antibodies (not depicted) and is in agreement with previous observations (Andreassen et al., 1998). These data imply that PP1α and -γ preferentially interact with distinct targeting subunits throughout the cell cycle and hence play distinct roles.

We thus sought to identify proteins that associate preferentially with either FP-PP1α or FP-PP1γ by immunoprecipitating the fusion proteins from interphase nuclear lysates using the same anti-GFP antibody. Although this approach was not likely to identify mitosis-specific targeting proteins (i.e., those that only bind PP1 during mitosis), we made the assumption, based on known regulatory roles for PP1 in transcription and chromatin remodeling (for review see Ceulemans and Bollen, 2004), that the chromatin targeting of PP1γ at anaphase was maintained into the following interphase. No clear differences were detected when immunoprecipitates were screened by SDS-PAGE separation and silver staining (Fig. 1 F). However, a far Western assay using in vitro–translated ^{35}S-labeled PP1 offered a means to directly detect and compare the subset of proteins coprecipitated with FP-PP1α (Fig. 1 G, lane 2) and FP-PP1γ (lane 3), which bind directly to the phosphatase. This revealed differences in the proteins that coprecipitated with the respective isoforms (Fig. 1 G, arrowheads). Immunoprecipitation of unfused FP from the HeLa^{EGFP} cell line, using the same anti-GFP antibody, coprecipitated little or no PP1 binding proteins, confirming the specificity of these interactions (Fig. 1 G, lane 1).

Combined SILAC/proteomic analysis of PP1-interacting proteins

A SILAC proteomic analysis was performed to identify and quantify the proteins that immunoprecipitate with anti-GFP antibodies from HeLa^{EGFP}, HeLa$^{EGFP\text{-}PP1\alpha}$, and HeLa$^{EGFP\text{-}PP1\gamma}$ cell lines (Fig. 2 A). Sample peptide spectra are shown for three proteins, each with a different arginine ratio (Fig. 2, B–D). Contaminating proteins that copurify with FP alone as well as with the FP-PP1 fusion proteins show an arginine ratio of 1:1:1 (hnRNP K; Fig. 2 B), whereas proteins that copurify specifically with either FP-PP1α (NIPP1; Fig. 2 C) or FP-PP1γ (Q69YH5; Fig. 2 D) have ratios reflecting this enrichment for

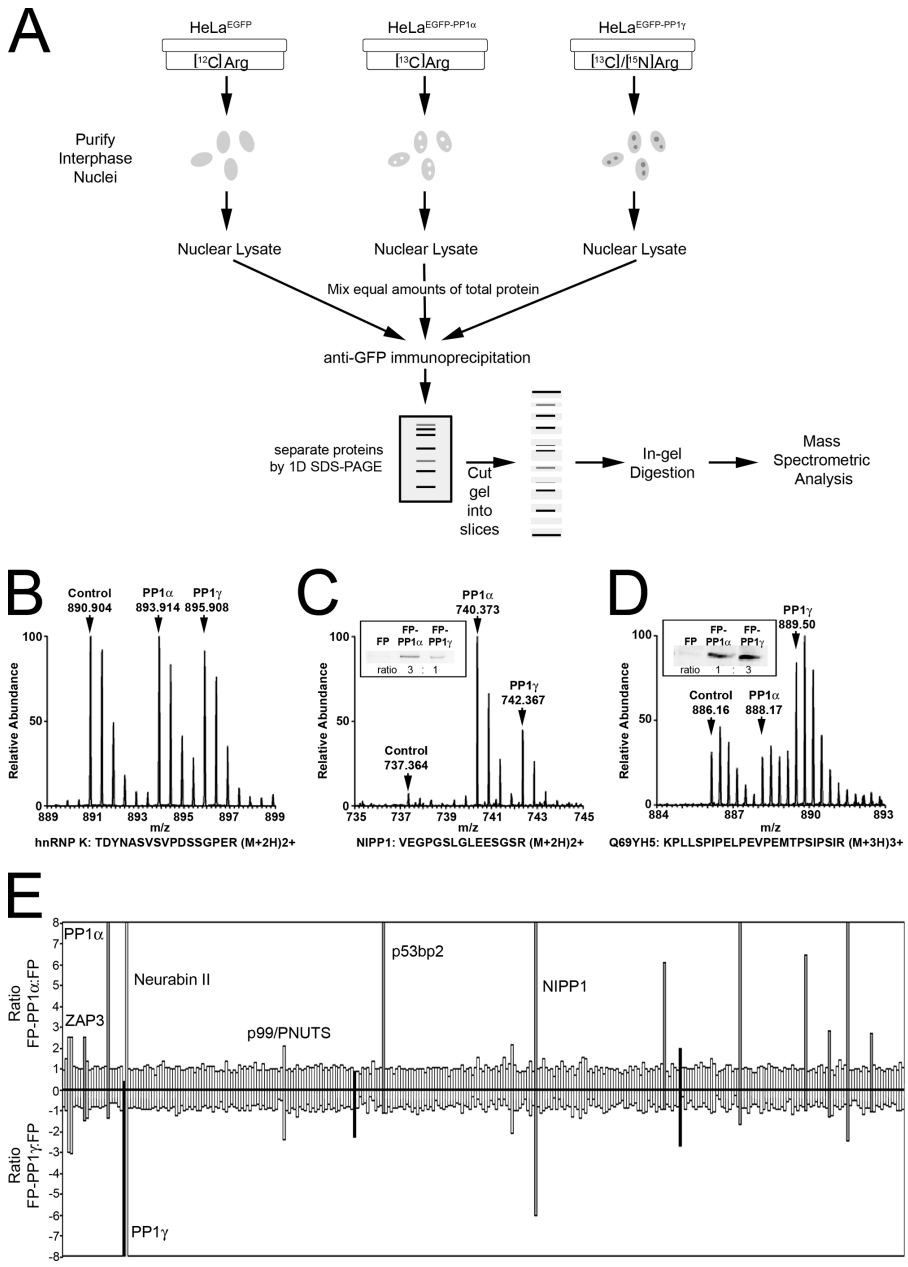

Figure 2. **Identification of PP1 binding proteins by combined SILAC/mass spectrometry.** (A) Design of the SILAC experiment. (B–D) Sample peptide spectra measured, illustrating the shift in peptide mass caused by incorporation of heavy arginine isotopes. Proteins that copurify with FP, FP-PP1α, and FP-PP1γ show a 1:1:1 ratio (B). Proteins showing specific interactions with either FP-PP1α (C) or FP-PP1γ (D) reflect that in their arginine ratios, which are in agreement with those calculated by quantitation of protein levels via Western blotting (C and D, insets). (E) Proteins identified in one experiment, listed in order of database identification score and plotted as relative abundance ratios (FP-PP1α/FP plotted as positive values and FP-PP1γ/FP plotted as negative values). Ratios >1.5 are taken to indicate specific coimmunoprecipitation with FP-PP1. PP1α and -γ peptides were also found, with the expected arginine ratios for their respective cell lines.

heavier forms of arginine. The accuracy of this mass spectrometric approach was confirmed by Western blot analyses for both NIPP1 (Fig. 2 C, inset) and Q69YH5 (Fig. 2 D, inset).

Quantified proteomic data obtained for the full spectrum of proteins identified in this screen are presented in the graph in Fig. 2 E, in which the mean arginine isotope ratio of FP-PP1 to FP for all quantifiable peptides is plotted for each protein. To facilitate visual comparison, the ratio is shown as a positive value for FP-PP1α and a negative value for FP-PP1γ. It is clear that although most of the proteins are not specific PP1-interacting factors and also copurify with FP alone (ratios ∼1), several proteins show enhanced copurification with FP-PP1 (ratios >1.5), and several of these show a preference for one of the isoforms. The large fraction of copurifying proteins revealed by isotope labeling to be contaminants prompted us to add a selective elution step with an RVXF motif–containing peptide that displaces proteins bound to PP1 via this motif (data included in Table S1, available at http://www.jcb.org/cgi/content/full/jcb.200508154/DC1). However, although this reduced the number of proteins recovered by ∼50%, the resulting protein mixture still contained a large fraction of contaminants, illustrating the utility of the isotope-labeling method and the importance of including the unfused FP internal control. The PP1-interacting factors revealed by the isotope labeling as specific (ratio >1.5) are listed in Table I and include known PP1 binding proteins as well as multiple novel factors, a subset of which contains an RVXF motif and is thus likely to bind PP1 directly. Factors lacking this motif may bind PP1 by another mechanism or may represent indirectly associated proteins that are part of larger PP1 complexes. A comprehensive list of all copurifying proteins identified, including contaminants, is provided in Table S1.

Table I. **PP1-interacting proteins identified by combined SILAC/proteomics**

Accession number	Protein name	Isoform preference	Molecular mass	Number of unique peptides quantified	Canonical RVXF motif	References
			kD			
Known PP1 binding proteins						
P49750	ZAP3	None	219.9	50	+	Tran et al., 2004
Q75MG7	KPI-2	PP1γ	164.9	2	+	Wang and Brautigan, 2002
Q13625	p53bp2	PP1α	125.6	13	+	Helps et al., 1995
Q96QC0	P99/PNUTS	PP1α	99.1	9	+	Kreivi et al., 1997; Allen et al., 1998
Q96SB3	Neurabin II/ Spinophilin	None	89.5	21	+	Hsieh-Wilson et al., 1999
Q12972	NIPP1	PP1α	38.5	8	+	Van Eynde et al., 1995; Trinkle-Mulcahy et al., 1999
Novel PP1-interacting proteins						
Q9H9B9	RIF1, isoform 4	PP1α	274.6	9	+	—
Q5VV35	Myopalladin	PP1α	145.3	3	+	—
Q69YH5	Repo-Man	PP1γ	112.7	4	+	—
Q01844	EWS	PP1α	68.5	3	+	—
Q68CK8	KIAA1949	PP1α	67.9	4	+	—
O94842	LCP1	PP1γ	66.2	1	−	—
Q8NCH2	FLJ90254	PP1α	47.3	4	+	—
Q6ZUJ6	FLJ43651	PP1α	42.8	8	−	—
Q6UXN9	WD40	None	35.2	5	−	—

Q69YH5, a novel PP1γ-specific interacting protein

We were particularly interested in proteins showing preferential interaction with PP1γ, with the aim of identifying the mechanism through which this isoform specifically localizes to chromatin. One of the novel proteins found to interact preferentially with PP1γ contained a canonical RVXF motif, suggesting it was a good candidate for further analysis. This protein, Q69YH5, whose function is unknown, copurified with PP1γ in a 3:1 ratio over PP1α (Fig. 2 D).

Analysis of the sequence of Q69YH5 revealed stretches of basic residues upstream and acidic residues downstream of the RVXF motif, which have been shown to enhance interaction with PP1 (Zhao and Lee, 1997). Q69YH5 is a unique protein with homologues in vertebrates but apparently not in lower eukaryotes. The region surrounding the RVXF motif is particularly conserved among vertebrate species (Fig. 3 B; see Fig. S1, available at http://www.jcb.org/cgi/content/full/jcb.200508154/DC1, for a full sequence alignment). The human gene is located at chromosome 8p21.2, and Northern blot analysis suggests that it is ubiquitously expressed (GeneNote; http://genecards.weizmann.ac.il/genenote).

To aid the molecular characterization of Q69YH5, we raised antibodies against peptides from both the NH_2 and COOH termini (Fig. 3 A). Both antibodies recognize a protein of the expected molecular mass (~113 kD) for the endogenous Q69YH5 in HeLa nuclear extracts (Fig. 4 A) and detect appropriately sized bands when tagged derivatives are exogenously expressed (Fig. S2, available at http://www.jcb.org/cgi/content/full/jcb.200508154/DC1). We note that the antibody raised against the NH_2-terminal peptide recognized an additional band in HeLa extracts of ~65 kD, which has not been characterized further.

Characterization of endogenous and tagged Q69YH5

Using the anti-peptide antisera, we confirmed that endogenous Q69YH5 interacts with PP1 in vivo. Affinity-purified anti-Q69YH5 antisera coimmunoprecipitated PP1γ from HeLa interphase nuclear lysate (Fig. 4 B, lane 3), and this coimmunoprecipitation was lost when the antibody was preincubated with the cognate peptide (Fig. 4 B, lane 4). Purification of endogenous PP1 complexes from interphase nuclear lysates using microcystin affinity chromatography also verified that endogenous Q69YH5 (Fig. 4 C, lane 2) is in a complex with PP1. Using HeLa cell fractions, we showed that endogenous Q69YH5 is predominantly nuclear (Fig. 4 A). This was confirmed by immunostaining paraformaldehyde-fixed HeLa cells with anti-Q69YH5, which revealed a widespread nucleoplasmic accumulation of the protein, largely excluding nucleoli (Fig. 4 D). This staining pattern was lost upon preincubation of the antibody with the cognate peptide (unpublished data). Interestingly, immunolocalization of Q69YH5 in mitotic cells showed a diffuse pattern in metaphase (Fig. 4 E) and an enhanced accumulation on chromatin at anaphase and telophase (Fig. 4, F and G, arrowheads). This was similar to the distribution seen for PP1γ and encouraged us to examine the dynamic behavior of Q69YH5 in live cells.

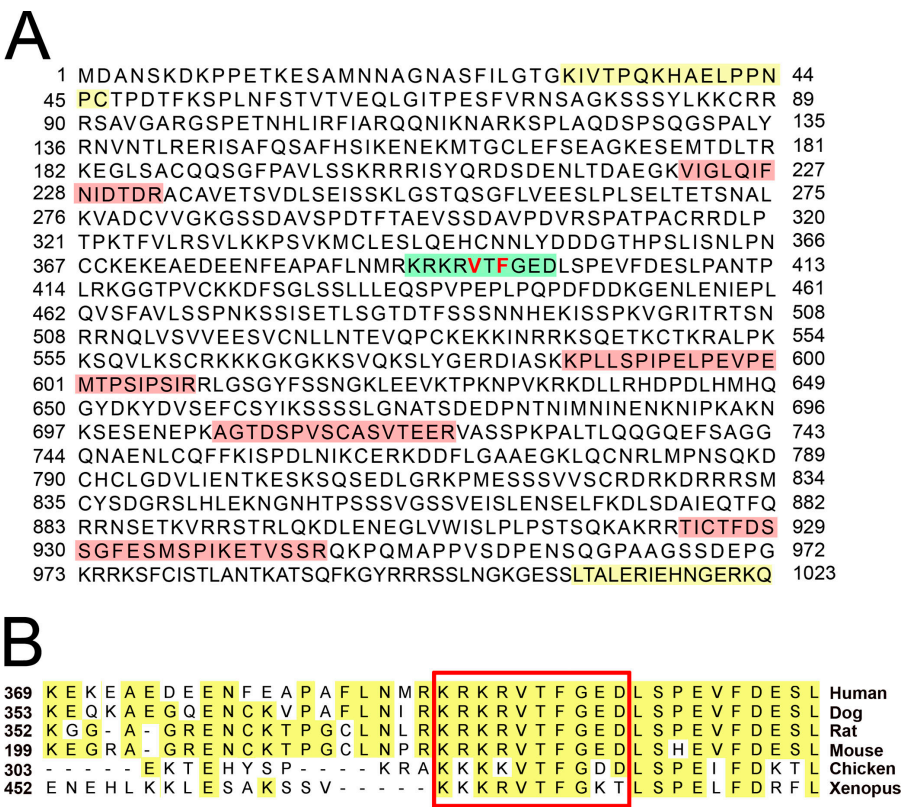

Figure 3. **Sequence analysis of Q69YH5.** (A) Amino acid sequence for Q69YH5, highlighting peptides identified by mass spectrometry (pink), peptides used to raise affinity-purified antibodies (yellow), and the putative RVXF (PP1 binding) motif (green). For mutational analysis, the hydrophobic Val and Phe residues within this region (red) were mutated to Ala. (B) Clustal alignment of this region in Q69YH5 protein sequences from several vertebrates. Identical residues are highlighted in yellow, and the highly conserved RVXF motif is outlined in red. The full sequence alignment is shown in Fig. S1, available at http://www.jcb.org/cgi/content/full/jcb.200511068/DC1.

We therefore fused the Q69YH5 cDNA with EGFP and performed time-lapse imaging of FP-Q69YH5 transiently expressed in HeLa cells. Although a nucleoplasmic localization pattern similar to that observed for endogenous Q69YH5 is maintained throughout the G1, S, and G2 stages of the cell cycle, it changes dramatically at M phase (Fig. 4 H). The protein initially becomes diffuse throughout the cell as the nuclear membrane breaks down, and a faint accumulation is seen later on metaphase chromatin (Fig. 4 H, arrow). As the cell progresses to anaphase, there is a large accumulation of FP-Q69YH5 on chromatin (Fig. 4 H, box). Parallel time-lapse analysis of HeLa$^{EGFP\text{-}PP1\gamma}$ cells indicates that the timing of this chromatin association of FP-Q69YH5 coincides with that of FP-PP1γ (Fig. 4 I, box). These data, along with further characterization of the PP1 interaction, strongly indicate that Q69YH5 acts as a targeting subunit to recruit PP1 to chromatin at anaphase. We have therefore named Q69YH5 Repo-Man, for recruits PP1 onto mitotic chromatin at anaphase, to reflect this function.

Repo-Man has an essential cellular function

Having established that Repo-Man is recruited onto chromatin at anaphase and maintained there throughout interphase, we next addressed whether it is required for cell viability by reducing its levels using RNA interference (RNAi) knockdown. Four RNA duplexes targeted against Repo-Man were transiently transfected into HeLa cells, and the cells were monitored over time for viability, cell cycle progression, and levels of endogenous Repo-Man. As shown in Fig. 5, two of the Repo-Man duplexes caused a >80% reduction in protein levels by 24 h after transfection (Fig. 5 A), and this reduced protein level was maintained for a further 24 h, with levels only starting to rise again 72 h after transfection. The remaining two duplexes caused a smaller reduction in protein levels (~30%). As a negative control, cells were transfected with a nonspecific scrambled duplex (Fig. 5 A). A duplex targeting lamin A/C was used as a positive control for the transfection, causing a sustained reduction (>80%) in lamin A/C protein levels by 48 h after transfection (Fig. 5 A).

Cell cycle progression was also monitored over time by FACS analysis in cells transfected with Repo-Man duplex 1. Although there was a massive reduction in cell number over time after uptake of Repo-Man duplex versus scrambled (see the end of the paragraph), no significant differences were observed in cell cycle distribution patterns (Fig. 5, B–D, vs. Fig. 5 E), suggesting that cells are dying regardless of cell cycle stage. A prominent sub-G1 peak is observed from 48 h after transfection onwards for cells treated with the Repo-Man duplex (Fig. 5, C and D), indicating an accumulation of apoptotic cells. This peak was not observed in cells treated with scrambled duplex, even at 72 h after transfection (Fig. 5 E). The small number of cells recovered after 72 h of Repo-Man knockdown (Fig. 5 D) compared with 72 h of treatment with scrambled duplex (Fig. 5 E) is consistent with a reduction in cell viability when Repo-Man levels are low (note the differences in scale in y axes).

Apoptosis of Repo-Man–depleted cells was confirmed by counterstaining with Annexin V–FITC and propidium iodide 24 h after transfection. At this stage, Annexin V binds to the externalized phosphatidyl serine characteristic of apoptotic cells, but propidium iodide is excluded because membrane integrity remains intact. Cells treated with the scrambled duplex did not

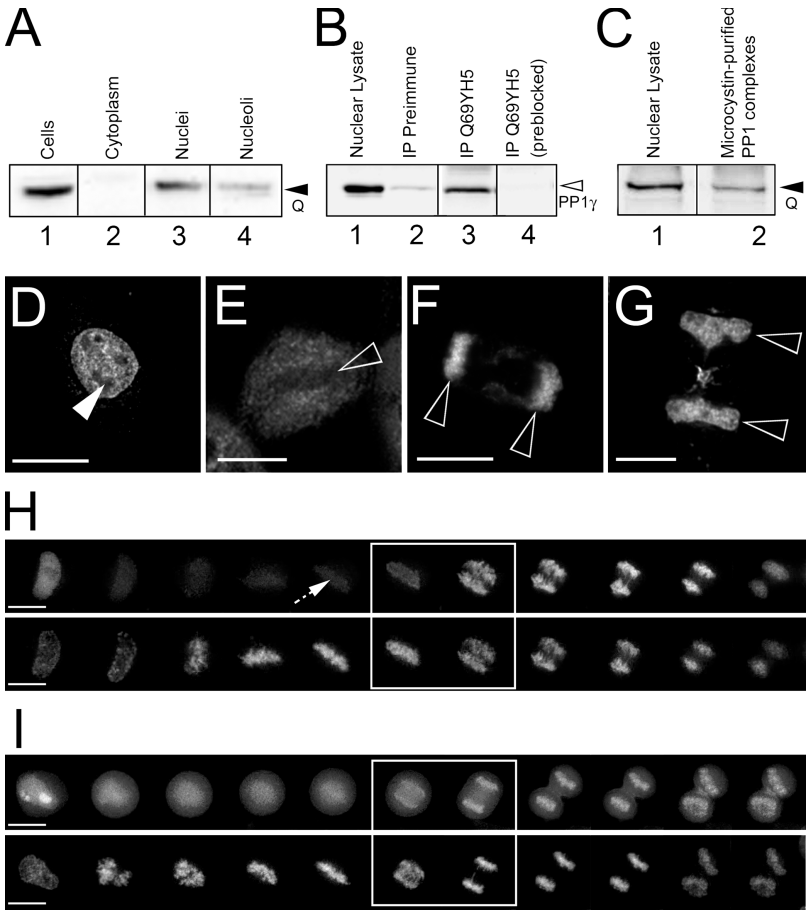

Figure 4. **Q69YH5 interacts with endogenous PP1 and localizes to chromatin.** (A) Western blot of HeLa cell fractions with anti-Q69YH5 peptide antibodies shows that Q69YH5 is a predominantly nuclear protein (lane 3, arrowhead). (B) When immunoprecipitated from interphase nuclear lysates, endogenous Q69YH5 coprecipitates endogenous PP1γ (lane 3, arrowhead). PP1 does not coprecipitate significantly with preimmune sera (lane 2) or with anti-Q69YH5 antibody pretreated with the cognate peptide (lane 4). (C) Purification of endogenous PP1 complexes from interphase nuclear lysates using microcystin affinity chromatography also shows that endogenous Q69YH5 (lane 2, arrowhead) is in a complex with PP1. (D–G) Staining of endogenous Q69YH5 with anti-Q69HY5 antibody reveals that is predominantly nucleoplasmic and excluded from nucleoli (closed arrowhead) during interphase (D). Q69YH5 is predominantly diffuse in metaphase cells (E) but shows an accumulation on chromatin (open arrowheads) during anaphase (F) and telophase (G). (H) This dynamic localization was confirmed by time-lapse imaging of HeLa cells transiently expressing FP-Q69YH5 (top) stained with Hoechst 33342 (bottom). Images were taken every 3 min as the cell progressed from prophase to telophase. There is a faint accumulation of FP-Q69YH5 on chromatin at metaphase (arrow). (I) For comparison, a similar time-lapse profile is shown for a HeLa$^{EGFP\text{-}PP1\gamma}$ cell (top) stained with Hoechst 33342 (bottom). The white boxes indicate the time at which a significant recruitment of both FP-Q69YH5 and FP-PP1γ onto chromatin is observed. Bars, 10 μm.

show any significant Annexin V staining or propidium iodide incorporation (Fig. 5 F), whereas a high proportion of cells treated with Repo-Man duplex 1 bound Annexin V, and the majority of these cells did not incorporate propidium iodide (Fig. 5 G). This indicated that membrane integrity was intact and that cells were therefore in an early stage of apoptosis. Further analysis of the mode of cell death during the 24–48-h time period was done by time-lapse imaging of cells transfected with either scrambled duplex or Repo-Man duplex 1, monitoring cells both by differential interference contrast (DIC) and by fluorescence imaging of Hoechst 33342–stained DNA for the characteristic membrane blebbing and nuclear fragmentation observed in apoptosis. The graph in Fig. 5 H sums up the scored results, with >60% of cells apoptosing in interphase after uptake of Repo-Man duplex 1. Less than 3% of these cells divide successfully over this time period, which explains why so few mitotic cells are observed in these knockdown experiments.

A soft agar colony–forming assay was also performed to assess cell viability. At 24 h after transfection, cells treated with either scrambled duplex or Repo-Man duplex 1 were transferred to the soft agar matrix at a clonal dilution. After 2 wk, there was a >50-fold difference in the number of colonies formed from cells treated with the scrambled duplex (Fig. 5 G, arrows) as compared with cells treated with the Repo-Man duplex (Fig. 5 I). In summary, the data show that RNAi-induced reduction in Repo-Man levels promotes the onset of apoptosis within 24 h and severely reduces cell viability.

PP1 binding and chromatin recruitment are separable properties of Repo-Man

To characterize the interaction of Repo-Man with PP1 in more detail and to address whether this activity is linked with its chromatin binding, we analyzed a Repo-Man mutant in which the two conserved hydrophobic residues within the putative PP1 binding domain were changed to alanine residues (i.e., RVXF to RAXA; Fig. 3 A). Transient overexpression of this mutant FP–Repo-Man (Fig. 6 B) showed that it had a localization similar to that of wild-type FP–Repo-Man (Fig. 6 A). Although both express at similar levels when transiently transfected into HeLa cells (not depicted), Western blotting reveals that only the wild type coprecipitates endogenous PP1γ (Fig. 6 C, lane 3), indicating that interaction with PP1 has been disrupted by mutation of this RVXF region.

We further tested the interaction of wild-type and RAXA mutant FP–Repo-Man with PP1γ by titrating varying levels of wild-type and mutant plasmid into HeLa$^{EYFP\text{-}PP1\gamma}$ cells. Under normal conditions during interphase, PP1γ is found in various cytoplasmic and nucleoplasmic pools, along with a prominent nucleolar accumulation (Fig. 1 E), whereas Repo-Man is nucleoplasmic (Fig. 6 A). When high levels of wild-type FP–Repo-Man are overexpressed, however, the cytoplasmic and nucleolar pools of PP1γ are greatly diminished and the majority of the protein shows a similar nucleoplasmic distribution to Repo-Man as it is retargeted by the expressed protein. In contrast, overexpression of RAXA mutant FP–Repo-Man, which does not bind PP1 (Fig. 6 C), fails to relocalize PP1γ. This is best illustrated

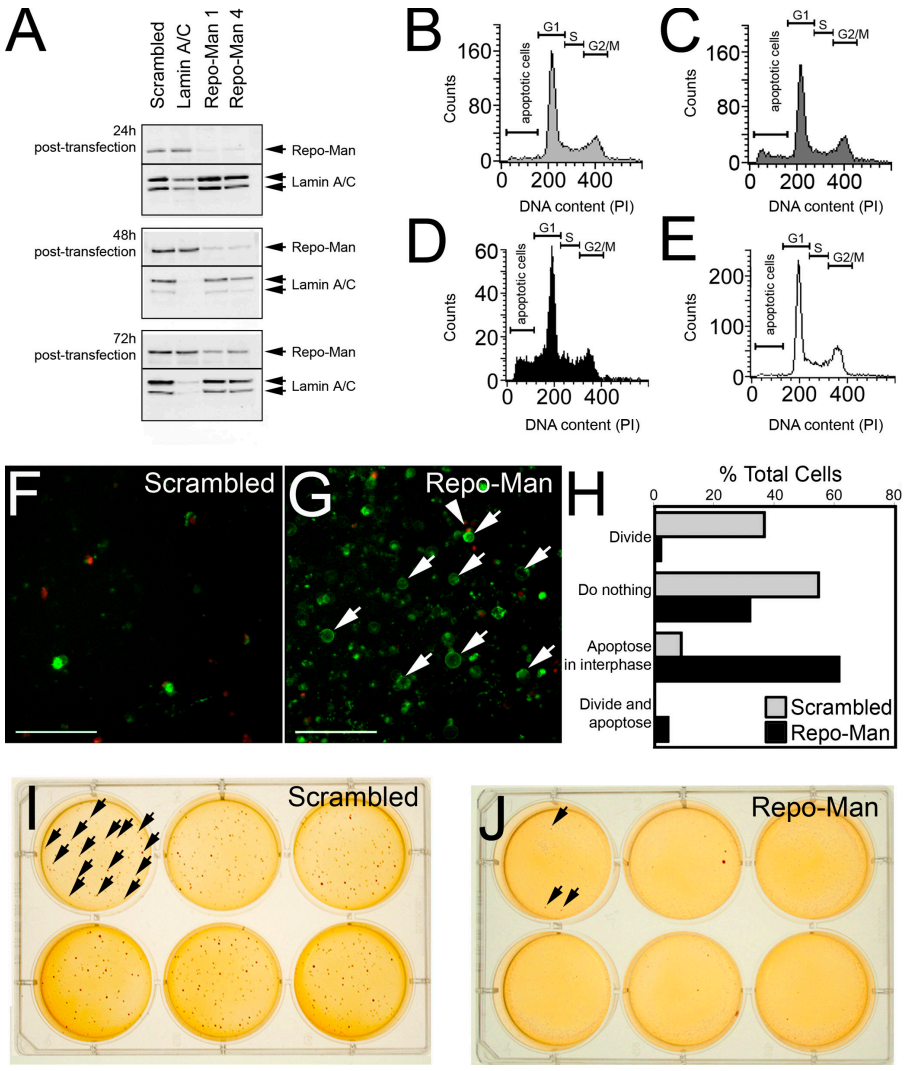

Figure 5. **Depletion of Repo-Man by RNAi induces apoptosis and decreases cell viability.** (A) Western blot analyses of HeLa cells treated with various siRNA duplexes. Lysates were prepared 24, 48, and 72 h after transfection. (B–D) FACS profiles for cells treated with Repo-Man duplex 1 and fixed at 24 h (B), 48 h (C), and 72 h (D) after transfection. (E) For comparison, a FACS profile for cells treated with scrambled duplex and fixed at 72 h is shown. (F and G) Cells treated with either scrambled duplex (F) or Repo-Man duplex 1 (G) for 24 h were also stained with Annexin V–FITC (green, arrows) and propidium iodide (red, arrowheads) to detect cells in early stages of apoptosis. Bars, 40 μm. (H) Graph summarizes the fates observed for HeLa cells by DIC imaging 24–48 h after transfection with either scrambled duplex (gray bars; $n = 90$) or Repo-Man duplex 1 (black bars; $n = 88$). The graph shows the number of cells in each category as a percentage of total cells. (I and J) Soft agar assays were performed to detect cell viability via colony formation (arrows) 2 wk after transfection with either scrambled duplex (I) or Repo-Man duplex 1 (J).

by comparing the localization of FP-PP1γ, which is exclusively nucleoplasmic at a 100:1 ratio of transfected wild-type to mutant Repo-Man expression plasmid, with the characteristic nucleolar accumulation of PP1γ seen at a 1:100 ratio of the same plasmids (Fig. 6 D). When both wild-type and mutant Repo-Man are overexpressed equally, an intermediate effect is observed. Thus, the ability of Repo-Man to influence PP1 localization in a concentration-dependent manner critically depends on the presence of a functional PP1-interaction domain. We conclude that Repo-Man, which binds directly to PP1 and influences localization, has the properties of a classic PP1-targeting subunit.

During mitosis, both PP1γ and Repo-Man simultaneously relocalize to chromatin at anaphase, which is most clearly illustrated by time-lapse fluorescence imaging of HeLa cells coexpressing FP-PP1γ and FP–Repo-Man (Fig. 7, A and B). Using a relocalization assay involving FP-PP1α, which does not accumulate on chromatin at anaphase (Fig. 1 H), it was shown that Repo-Man is directly involved in recruitment of PP1 to chromatin. Increased levels of exogenous FP–Repo-Man caused an ectopic recruitment of PP1α to chromatin at anaphase (Fig. 7, C and D). Interestingly, this accumulation of Repo-Man on chromatin appears to be independent of its ability to bind PP1. In cells expressing both FP-PP1α and RAXA mutant FP–Repo-Man, the mutant Repo-Man accumulates on chromatin as normal, whereas FP-PP1α retains its typical mitotic localization pattern (Fig. 7, E and F). We conclude that Repo-Man is a targeting subunit that recruits PP1 to chromatin and that this recruitment occurs initially at the metaphase–anaphase transition during mitosis. Interestingly, overexpression of both wild-type and mutant Repo-Man severely reduced both the total cell population and the number of mitotic cells observed, suggesting a deleterious effect on interphase cell function and/or entry into mitosis. It is therefore difficult to assess the possible mitotic defects associated with these perturbations, although we have found some evidence for chromosome condensation and segregation defects in cells overexpressing wild-type Repo-Man (Fig. S2).

RAXA mutant FP–Repo-Man acts as a dominant negative to displace Repo-Man–PP1γ complexes from chromatin

As noted in the previous paragraph, the RAXA mutant of FP– Repo-Man accumulates on chromatin in a fashion similar to wild type but no longer recruits PP1. The binding of Repo-Man to chromatin is reversible, as shown by FRAP analysis (Fig. S2).

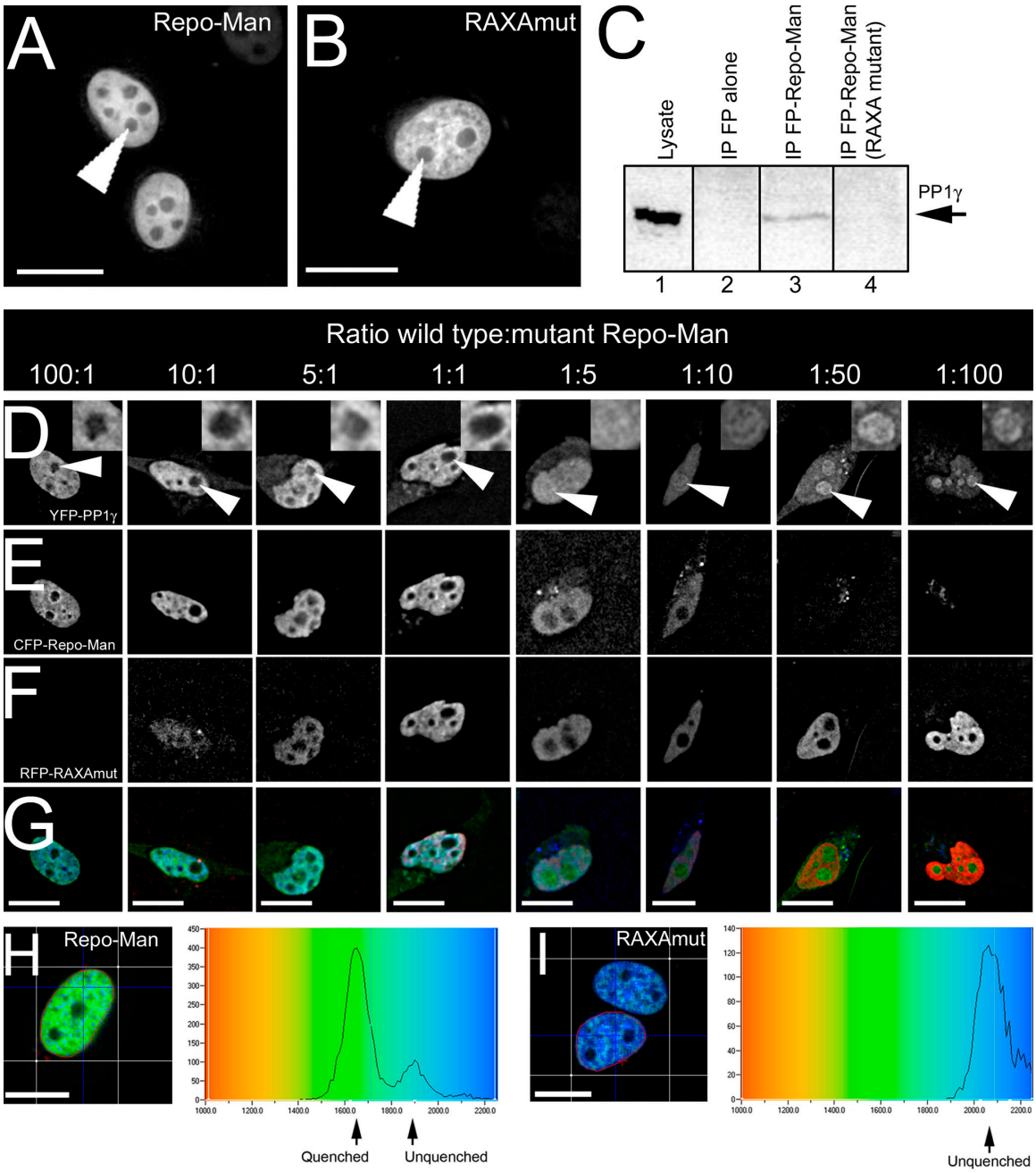

Figure 6. **Mutation of the RVXF motif in Repo-Man disrupts interaction with PP1.** (A and B) When transiently expressed, RAXA mutant FP–Repo-Man (B) shows a similar nucleoplasmic accumulation at interphase to wild type (A). Nucleoli are marked by arrowheads. (C) Unlike wild-type FP–Repo-Man (lane 3), the RAXA mutant does not coprecipitate endogenous PP1γ (lane 4), as shown by Western blotting. (D–G) Transient expression of wild-type but not RAXA mutant FP–Repo-Man also retargets exogenous PP1, as demonstrated by titrating varying levels of the two plasmids into HeLa$^{EYFP\text{-}PP1\gamma}$ cells. FP-PP1γ is shown in D (nucleoli indicated by arrowheads are enlarged in inset to compare PP1 levels), wild-type FP–Repo-Man in E, and RAXA mutant FP–Repo-Man in F. Merged images are shown in G. (H and I) A direct interaction is measured between wild-type CFP–Repo-Man and YFP-PP1γ using fluorescence lifetime imaging microscopy/FRET analysis (H) but not between RAXA mutant CFP–Repo-Man and YPF-PP1γ (I). Color-coded fluorescence lifetime maps are shown for each CFP construct (donor) in the presence of YFP-PP1γ (acceptor) and the respective quenched and unquenched lifetimes indicated on the graphs. Bars, 10 μm.

If a limited number of binding sites exist, we would predict that expression of high levels of RAXA mutant Repo-Man could displace endogenous Repo-Man–PP1 complexes on chromatin. To test this, we compared the anaphase chromatin targeting of FP-PP1γ in the presence of high levels of exogenously expressed RAXA mutant FP–Repo-Man (Fig. 8, C and D) to that observed normally (Fig. 8, A and B). A reduced accumulation of FP-PP1γ on chromatin was evident (Fig. 8, A–D, arrowheads), as compared with cells not expressing the mutant Repo-Man, and we therefore propose the displacement model shown in Fig. 8 E. However, we note that almost no mitotic cells and relatively few interphase cells were detected expressing very high levels of RAXA mutant FP–Repo-Man, indicating that it adversely affects cell viability (see the following paragraph). These data

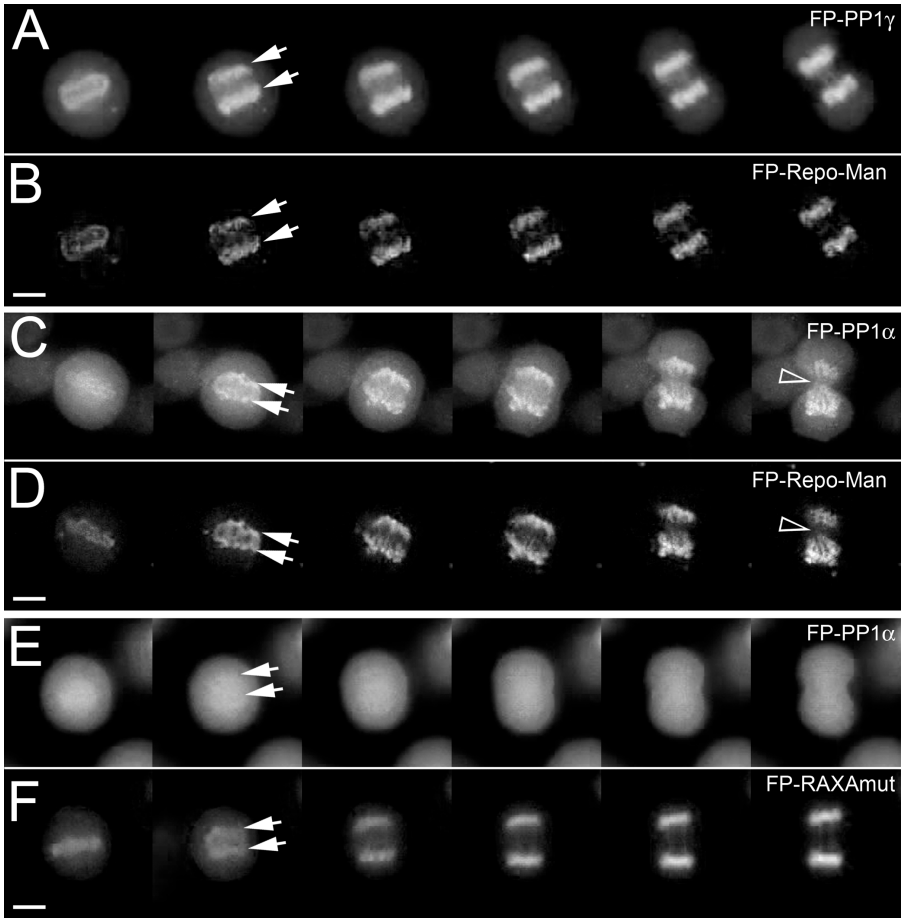

Figure 7. **Overexpression of FP–Repo-Man ectopically recruits FP-PP1α to chromatin.** (A and B) A series of time-lapse images taken every 3 min of a HeLa$^{EYFP\text{-}PP1\gamma}$ cell (A) transiently expressing ECFP–Repo-Man (B) as it progresses from metaphase to telophase. Arrows mark chromatin regions. (C and D) Time-lapse series for a HeLa$^{EGFP\text{-}PP1\alpha}$ cell transiently expressing monomeric dsRed–Repo-Man (D), which retargets a significant pool of FP-PP1α (C) to chromatin at anaphase (arrows) and retains it there. Note the lagging chromosomes observed under these conditions (arrowheads). (E and F) Expression of RAXA mutant FP–Repo-Man (F) does not cause this retargeting of FP-PP1α (E). Bars, 10 μm.

suggest that RAXA mutant Repo-Man can act as a dominant negative to displace endogenous Repo-Man–PP1γ complexes from chromatin during both anaphase and interphase.

The RNAi knockdown experiments (Fig. 5) showed that Repo-Man is important for cell viability. The dominant-negative effect of the RAXA mutant provided a means to determine whether the cellular requirement for Repo-Man was connected to its role as a PP1-interacting protein. To do this, we compared the level of cell death resulting from either mock-transfection or transfection with the dominant-negative RAXA mutant of Repo-Man. A much larger level of cell death was observed for cell populations expressing RAXA mutant FP–Repo-Man (Fig. 8, H and I). A more detailed inspection of the dying cells revealed that the majority of cell death occurred during interphase (Fig. 8 J, lane 3). We did not observe an obvious mitotic block, although a proportion of cells died either during or immediately after mitosis (Fig. 8 J, lanes 4 and 5). As noted in the previous paragraph, there was a severe reduction in the number of mitotic cells observed, which is in agreement with the rapid onset of apoptosis. These data strongly argue that the essential role of Repo-Man in cell viability is directly related to its PP1-targeting activity.

Discussion

Distinct pools of PP1 play different roles in the cell, mediated by the binding of a common catalytic subunit to different targeting proteins. In this study, we used a combination of time-lapse fluorescence imaging and a novel proteomics strategy to characterize targeting proteins that can bind differentially to the α and γ isoforms of PP1. Specifically, we observed a pool of chromatin-bound PP1γ that is first recruited at anaphase and identified the targeting protein responsible. The Repo-Man–PP1 complex is loaded onto chromatin at anaphase, where it remains during interphase and is subsequently displaced when cells enter prophase (Fig. 9). Further characterization of Repo-Man showed that perturbation of its PP1 binding or expression level caused a variety of cell defects, as discussed later in this section.

We adopted a mass spectrometric strategy involving differential stable isotope labeling, which allowed a quantitative comparison of the relative distribution of targeting subunits between the two PP1 isoforms and the ready elimination of nonspecific contaminants. The identification of Repo-Man was facilitated by the enhanced sensitivity available using this method. For example, Repo-Man was not detected in previous studies using affinity chromatography with immobilized microcystin, a cyclic peptide toxin that binds PP1 and PP2A covalently (Moorhead et al., 1994). However, we found that Repo-Man does copurify among the proteins binding endogenous PP1 that are enriched by microcystin chromatography from interphase nuclear lysates when we detect it using anti–Repo-Man antibodies (Fig. 4 C), suggesting it was previously

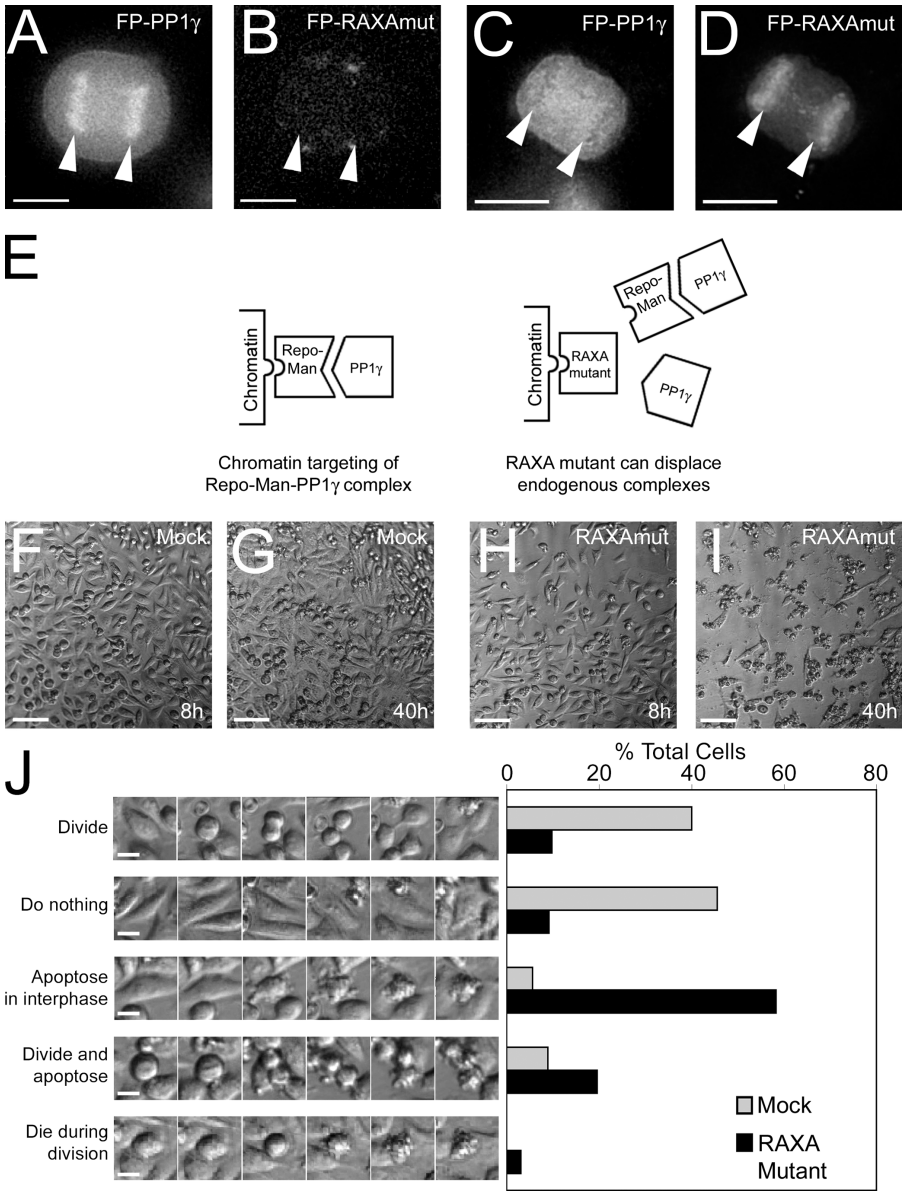

Figure 8. **Overexpression of RAXA mutant FP–Repo-Man displaces endogenous Repo-Man–PP1γ complexes from chromatin.** (A–D) When RAXA mutant FP–Repo-Man (D) is expressed in HeLa$^{EGFP\text{-}PP1\gamma}$ cells, significantly lower levels of FP-PP1γ (C) are found on anaphase chromatin (arrowheads), compared with the levels observed (A) in cells expressing little or no mutant FP–Repo-Man (B). Bars, 10 μm. This indicates a dominant-negative effect, as depicted by E. (F–I) Time-lapse DIC imaging of HeLa cells after mock-transfection (F and G) or transfection with RAXA mutant FP–Repo-Man (H and I) was used to quantify the extent and type of cell death caused by these conditions, between 8 h (F and H) and 40 h (G and I) after transfection. Bars, 100 μm. (J) Summary of the fates observed for HeLa cells by DIC imaging after either mock-transfection (gray bars; $n = 90$) or transfection with RAXA mutant monomeric dsRed–Repo-Man (black bars; $n = 163$). Cell fates were divided into five categories as indicated, and the graph shows the number of cells in each category as a percentage of total cells. Bars, 10 μm.

missed because of its relatively low abundance compared with other PP1 binding factors. In addition to offering increased sensitivity of detection, the SILAC approach also proved useful for identifying real PP1-specific proteins among the large number of copurifying contaminants. This aids identification of proteins that may be lost upon higher stringency purification strategies. Because as high as 90% of the copurified proteins proved to be contaminants (Fig. 2 E), the success of the strategy depended

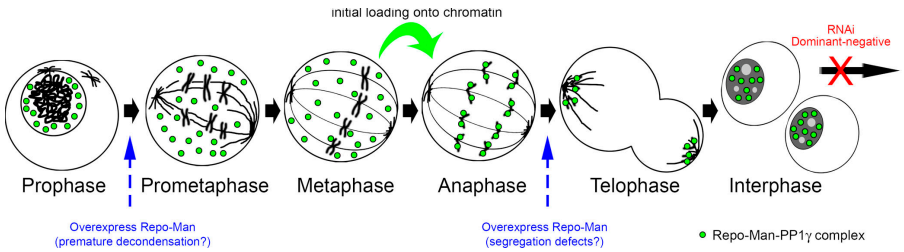

Figure 9. **Localization of Repo-Man–PP1γ complexes throughout the cell cycle.** Based on the data presented in this study, we provide a depiction of the localization of Repo-Man–PP1γ complexes (green) throughout the cell cycle, noting its initial loading onto chromatin at the metaphase–anaphase transition. Also shown is the key stage (red) at which both RNAi knockdown of endogenous Repo-Man and displacement of endogenous Repo-Man–PP1 complexes by the dominant-negative mutant induce apoptosis in interphase cells. Observed effects of overexpression of wild-type Repo-Man on mitotic cells are also indicated (blue).

on inclusion of an internal negative control (cells expressing the FP tag alone). Any putative interacting proteins not specific to PP1 contained equal amounts of $^{12}C/^{14}N$-labeled peptides (from the FP cell line) to heavy isotope-labeled peptides (from the FP-PP1 cell lines). Furthermore, the ratio of the $^{13}C/^{14}N$ to $^{13}C/^{15}N$-labeled peptides distinguished whether the targeting subunits bound preferentially to PP1α or -γ. Although we have applied this to the study of PP1, we envisage that a similar strategy could be adopted to analyze and quantitate the differential interactions of any closely related proteins or modified versions of the same protein, with binding partners in other biological systems.

Time-lapse fluorescence imaging of the respective FP-PP1 stable cell lines revealed that both FP-PP1α and FP-PP1γ localize to kinetochores in metaphase; however, PP1α appears to be predominantly excluded from other chromatin regions at this stage, in contrast to PP1γ. Furthermore, we observe a dramatic increase in the accumulation of FP-PP1γ on chromatin at anaphase, where it is retained as daughter nuclei reform. This differential binding to chromatin explains why FP-PP1α appears in daughter nuclei much later and indicates the existence of chromatin binding factors that can selectively target PP1γ. Our strategy of screening PP1 binding proteins for factors showing a preference for PP1γ thus enabled us to identify Repo-Man as a targeting subunit that mediates the regulated interaction of PP1γ with chromatin.

Repo-Man is a previously uncharacterized protein first detected as being a member of a group of proteins whose mRNA expression correlated with that of known cell cycle–related proteins (Walker, 2001). Interestingly, another of these proteins, borealin, has recently been identified as a novel chromosomal passenger protein required for stability of the bipolar mitotic spindle (Gassmann et al., 2004). More recently, Repo-Man was found among a group of cell cycle genes up-regulated in aggressive neuroblastoma tumors (Krasnoselsky et al., 2005). We show that Repo-Man is a chromatin binding factor that also associates with PP1 via the canonical RVXF motif.

Although the loading of Repo-Man–PP1γ complexes onto chromatin occurs dramatically at the onset of anaphase, several lines of evidence suggest that the proteins remain associated in a complex bound to chromatin during interphase. Direct biochemical and proteomic analysis of interphase nuclei showed that both endogenous and FP-tagged PP1 copurify with Repo-Man, and fluorescent resonance energy transfer (FRET) experiments confirm that PP1 and Repo-Man can interact directly during interphase (Fig. 6 H). It is important to note that although PP1γ shows a strong nucleolar accumulation during interphase, it represents only ∼20% of the total nuclear pool of PP1, with the remaining 80% in the nucleoplasm. The identity of the nucleolar targeting subunit for PP1γ remains unknown, but our present data indicate that Repo-Man, along with NIPP1, ZAP3, p99/PNUTS, and other proteins, is involved in targeting pools of PP1γ to different nucleoplasmic sites, including chromatin, during interphase. Further evidence supporting the persistence of the Repo-Man–PP1γ complex on chromatin during interphase comes from photobleaching studies, which show a similar turnover rate for nucleoplasmic Repo-Man in interphase nuclei compared with Repo-Man on mitotic chromosomes (Fig. S2). Based on the photobleaching data, it appears that the protein is released from chromatin in late prophase, remaining predominantly diffuse until its recruitment back on to chromatin first at low levels during metaphase and then more dramatically at the onset of anaphase. Western blotting analysis revealed no major differences in Repo-Man levels at different stages of the cell cycle (unpublished data), indicating that its accumulation on chromatin at anaphase results from relocalization of an existing pool and not new synthesis. It will be important to determine what controls this cell cycle–modulated association of Repo-Man with chromatin and whether it is a direct (e.g., covalent modification) or indirect (e.g., interaction with another factor) regulatory event.

Localization of PP1 to chromatin is in agreement with several of its known regulatory roles, which include dephosphorylation of histones and other mitotic phosphoproteins, regulation of chromosome decondensation and nuclear membrane assembly at the M–G1 transition, and regulation of both transcription and chromatin remodeling during interphase (for review see Ceulemans and Bollen, 2004). An important future goal, therefore, is the identification, by a similar SILAC/proteomic approach, of new binding partners for Repo-Man, which will provide clues to the specific regulatory pathways in which this PP1 complex is involved. Mapping the specific regions of Repo-Man required for chromatin localization will also facilitate the identification of binding partners and/or the mechanism of chromatin interaction, which was shown here to be separable from its PP1 binding ability.

Changes in expression levels of many cell cycle–regulated kinases and phosphatases have serious consequences for cell viability (Mackeigan et al., 2005). Similarly, we find that depletion of Repo-Man by RNAi knockdown leads to cell death by apoptosis, primarily in interphase. Overexpression of mutant Repo-Man that does not bind PP1 leads to a similar phenotype, suggesting that it is the loss of endogenous Repo-Man–PP1γ complexes from chromatin that initiates the apoptotic pathway, either directly or indirectly. There is no apparent mitotic block, and time-lapse imaging of chromatin in these cells does not provide any further clues to the disrupted pathway (Fig. S3, available at http://www.jcb.org/cgi/content/full/jcb.200508154/DC1). The very rapid onset (within 24 h) of apoptosis results in very few cells surviving into mitosis (Fig. 5 H and Fig. 8 J), making it difficult to assess the possible mitotic defects associated with these perturbations. For example, although analysis of large numbers of $HeLa^{EGFP\text{-}PP1\gamma}$ cells treated with Repo-Man duplex 1 revealed that, as in parental HeLa cells, the majority of cells die rapidly through apoptosis in interphase, only a few mitotic cells (<2% of the total population screened) could be found to confirm that FP-PP1γ no longer accumulates on chromatin at anaphase and telophase under these conditions (Fig. S3).

Overexpression of wild-type Repo-Man also promotes apoptosis but with lower efficiency. In the small proportion of cells surviving into mitosis, we observed evidence for chromosome segregation defects (Fig. S2). Collectively, the knockdown and overexpression data suggest that the Repo-Man–PP1γ complex may play important roles at multiple stages of the cell cycle,

including both interphase and mitosis. For example, Repo-Man may target PP1γ to dephosphorylate chromatin-associated factors, thus modulating their role in maintaining the degree of chromatin condensation throughout the cell cycle, which is critical for both cell division and viability. Additionally, the Repo-Man–PP1γ complex may play an important role in modulating chromatin accessibility or the activity of specific transcription factors during interphase. Disruption of this interphase role is the likely cause of the large-scale apoptosis observed upon knockdown of Repo-Man, whereas the chromosome segregation defects found upon overexpression of Repo-Man point to disruption of a mitotic regulatory role. Further work is therefore required to investigate the essential roles of the Repo-Man–PP1 complex throughout the cell cycle.

Materials and methods

Plasmids and antibodies

Repo-Man was cloned from expressed sequence tags (IMAGE clones 4803608 and 4838503; Geneservice Ltd.) using oligonucleotide primers, inserted into EGFP/EYFP/ECFP-C1 and monomeric dsRed-C1 FP vectors (Invitrogen) and confirmed by restriction analysis and DNA sequencing. The Val and Phe residues of the putative PP1 binding motif (residues 393 and 395) were changed to Ala using two-step recombinant PCR mutagenesis. Polyclonal antibodies were raised in rabbits against Repo-Man peptides (Fig. 3 A) and affinity purified using the cognate peptides (Eurogentec). Anti–lamin A/C, anti-PP1α, and anti-PP1γ antibodies were obtained from Santa Cruz Biotechnology, Inc., all HRP-conjugated secondary antibodies were obtained from Perbio Science, and microcystin-Sepharose was obtained from Upstate Biotechnology.

Stable cell lines

All FP-PP1 constructs and the HeLa$^{EGFP\text{-}PP1\gamma}$, HeLa$^{EYFP\text{-}PP1\gamma}$, and HeLa^{EGFP} stable cell lines were obtained as described previously (Trinkle-Mulcahy et al., 2001, 2003). The HeLa$^{EGFP\text{-}PP1\alpha}$ stable cell line was established in a similar manner. Characterization of expressed FP-PP1 and FACS analyses were performed as previously described (Trinkle-Mulcahy et al., 2001).

Live cell imaging

Cells were cultured in glass-bottomed dishes (WILLCO; Intracel) and mounted on a wide-field fluorescence microscope (DeltaVision Spectris; Applied Precision) fitted with an environmental chamber (Solent Scientific) to maintain temperature at 37°C and a CoolMax charge-coupled device camera (Roper Scientific). Before imaging, growth medium was replaced with Phenol Red-free CO_2 independent medium (Invitrogen). DNA was stained by incubating the cells for 30 min in medium containing 0.25 μg/ml Hoechst No. 33342 (Sigma-Aldrich). Cells were imaged using a 60× NA 1.4 Plan-Apochromat objective. For time-lapse imaging, five optical sections of 1 μM each were recorded every 3 min, with an exposure time of 0.1 s for EGFP and 0.05 s for Hoechst 33342. DIC imaging was obtained with the appropriate prism insert (Olympus). All fluorescence time-lapse images are presented as two-dimensional projections of the three-dimensional datasets. For high-resolution imaging, either 20 (interphase cells) or 40 (mitotic cells) optical sections of 0.5 μM each were collected, with exposure times of 0.5 s for EGFP. Similar settings were used to image ECFP- and EYFP-tagged proteins, using the appropriate filter sets (Chroma Technology Corp.). SoftWorX software (Applied Precision) was used for image acquisition, data deconvolution, and volume rendering. Fluorescence lifetime imaging microscopy/FRET experiments were performed on a fluorescent lifetime imaging system (Radiance 2100MP; Bio-Rad Laboratories).

Immunoaffinity purification of FP–PP1 complexes

Cells were grown for six cell divisions in L-arginine (HeLa^{EGFP}), L-arginine $^{13}C_6{}^{14}N_4$ (HeLa$^{EGFP\text{-}PP1\alpha}$), or L-arginine $^{13}C_6{}^{15}N_4$ (HeLa$^{EGFP\text{-}PP1\gamma}$) labeling media before purification. Nuclei were isolated from cells using a variation of a previously described technique (Andersen et al., 2002). Purified nuclei were resuspended in RIPA buffer to solubilize proteins. Lysates from each cell line were mixed in a 1:1:1 ratio based on total protein concentration, and FP proteins were affinity purified using anti-GFP monoclonal antibodies (Roche) covalently coupled to protein G–Sepharose, as previously described (Trinkle-Mulcahy et al., 2001). For the peptide elution experiment, the beads were incubated with an RVXF peptide from ZAP3 (sequence GKKRVRWADLE) to elute PP1-interacting proteins. Immunoprecipitated proteins were separated on NuPAGE 4–12% Bis-Tris gels and excised into 12 slices. Peptides resulting from in-gel digestion were extracted from the gel pieces, desalted, concentrated on reverse phase–C18 tips, and eluted into 96-well plates for automated mass spectrometric analysis.

For some experiments, the FPs from each nuclear lysate were affinity purified separately and subjected to one-dimensional SDS-PAGE, followed by silver staining or immunoblotting. For the far Western assays using ^{35}S-PP1, the substrate was prepared by in vitro translating PP1γ (in a pcDNA vector) in the presence of [^{35}S]methionine using the TNT T7 quick coupled transcription/translation system (Promega). Blots were blocked overnight with 10% milk powder in PBS, washed well with PBS, and incubated with ^{35}S-PP1 for 4 h. Additional PBS washes were performed before exposure to x-ray film to detect ^{35}S-PP1–labeled bands.

Mass spectrometry and data analysis

High-resolution mass spectrometric analysis was performed as described previously (Andersen et al., 2005) using the LTQ-FT-ICR mass spectrometer (Thermo Finnigan). Protein ratios were calculated for each arginine-containing peptide as the peak area of [^{13}C]Arg divided by the peak area of [^{12}C]Arg and the peak area of [^{13}C]/[^{15}N]Arg divided by the peak area of [^{12}C]Arg for each single scan mass spectrum. Peptide ratios for all arginine-containing peptides sequenced for each protein were averaged. MS-Quant, a software program developed in house, was used to extract information from the Mascot HTML database search files (Matrix Science) and to evaluate the certainty in peptide identification and in peptide abundance ratio. The program is available as open source at http://msquant.sourceforge.net.

RNAi

HeLa cells were transfected in 24-well plates with 1 μg of small interfering RNA (siRNA) duplexes (Dharmacon) using RNAiFect (QIAGEN) and either harvested or passaged 24 h after transfection.

Annexin V–FITC and soft agar assays

For the Annexin V–FITC assay, cells were grown and transfected with siRNA duplexes in 4-well chamber slides (Lab-Tek II; Nunc). After 24 h, the cells were stained using an Annexin V–FITC apoptosis detection kit (Abcam) and set up for live cell imaging.

For the soft agar assays, cells were grown and transfected with siRNA duplexes as described in the previous section and then trypsinized and mixed at a dilution of 4e^4 cell/ml with 0.3% agar in growth medium. This mixture was carefully pipetted onto 2 ml of base agar (0.5% agar in growth medium) in a 6-well plate at 0.5 ml/well and incubated at 37°C/5% CO_2 for 2 wk.

Online supplemental material

Table S1 contains a comprehensive list of all proteins identified in the SILAC/proteomic screen. Fig. S1 shows a Clustal alignment of Repo-Man protein sequences from several vertebrates. Fig. S2 shows Repo-Man detected by Western blotting, mitotic defects associated with its overexpression, and analysis of its turnover kinetics throughout the cell cycle. Fig. S3 shows DNA fragmentation induced by RNAi knockdown of Repo-Man and displacement of PP1γ from chromatin by overexpression of RAXA mutant Repo-Man. Video 1 shows a mitotic HeLa$^{EGFP\text{-}PP1\alpha}$ cell. Video 2 shows a mitotic HeLa$^{EGFP\text{-}PP1\gamma}$ cell. Video 3 shows FP-Q69YH5 transiently expressed in a mitotic HeLa cell stained with Hoechst 33342 to mark chromatin. Video 4 shows FP-PP1γ in a mitotic HeLa$^{EGFP\text{-}PP1\gamma}$ stained with Hoechst 33342 to mark chromatin. Video 5 shows a mitotic HeLa$^{EGFP\text{-}PP1\gamma}$ cell transiently expressing ECFP–Repo-Man. Video 6 shows a mitotic HeLa $^{EGFP\text{-}PP1\alpha}$ cell transiently expressing monomeric dsRed–Repo-Man. Video 7 shows a mitotic HeLa$^{EGFP\text{-}PP1\alpha}$ cell transiently expressing RAXA mutant monomeric dsRed–Repo-Man. Video 8 shows a field of HeLa cells mock-transfected and imaged 8–40 h after transfection. Video 9 shows a field of HeLa cells transfected with RAXA mutant FP–Repo-Man and imaged 8–40 h after transfection. Online supplemental material is available at http://www.jcb.org/cgi/content/full/jcb.200508154/DC1.

We would like to thank Dr. Sam Swift and the Light Microscopy Facility at the University of Dundee.

This work was funded by a Wellcome Trust Programme Grant (073980/Z/03/Z). A.I. Lamond is a Wellcome Trust Principal Research Fellow.

Work at the Centre for Experimental Bioinformatics is supported by a generous grant from the Danish National Research Foundation.

Submitted: 23 August 2005
Accepted: 17 January 2006

References

Allen, P.B., Y.G. Kwon, A.C. Nairn, and P. Greengard. 1998. Isolation and characterization of PNUTS, a putative protein phosphatase 1 nuclear targeting subunit. *J. Biol. Chem.* 273:4089–4095.

Andersen, J.S., C.E. Lyon, A.H. Fox, A.K. Leung, Y.W. Lam, H. Steen, M. Mann, and A.I. Lamond. 2002. Directed proteomic analysis of the human nucleolus. *Curr. Biol.* 12:1–11.

Andersen, J.S., Y.W. Lam, A.K. Leung, S.E. Ong, C.E. Lyon, A.I. Lamond, and M. Mann. 2005. Nucleolar proteome dynamics. *Nature.* 433:77–83.

Andreassen, P.R., F.B. Lacroix, E. Villa-Moruzzi, and R.L. Margolis. 1998. Differential subcellular localization of protein phosphatase-1 α, γ1, and δ isoforms during both interphase and mitosis in mammalian cells. *J. Cell Biol.* 141:1207–1215.

Blagoev, B., S.E. Ong, I. Kratchmarova, and M. Mann. 2004. Temporal analysis of phosphotyrosine-dependent signaling networks by quantitative proteomics. *Nat. Biotechnol.* 22:1139–1145.

Ceulemans, H., and M. Bollen. 2004. Functional diversity of protein phosphatase-1, a cellular economizer and reset button. *Physiol. Rev.* 84:1–39.

Cohen, P.T. 2002. Protein phosphatase 1–targeted in many directions. *J. Cell Sci.* 115:241–256.

de Hoog, C.L., and M. Mann. 2004. Proteomics. *Annu. Rev. Genomics Hum. Genet.* 5:267–293.

Egloff, M.P., D.F. Johnson, G. Moorhead, P.T. Cohen, P. Cohen, and D. Barford. 1997. Structural basis for the recognition of regulatory subunits by the catalytic subunit of protein phosphatase 1. *EMBO J.* 16:1876–1887.

Gassmann, R., A. Carvalho, A.J. Henzing, S. Ruchaud, D.F. Hudson, R. Honda, E.A. Nigg, D.L. Gerloff, and W.C. Earnshaw. 2004. Borealin: a novel chromosomal passenger required for stability of the bipolar mitotic spindle. *J. Cell Biol.* 166:179–191.

Helps, N.R., H.M. Barker, S.J. Elledge, and P.T. Cohen. 1995. Protein phosphatase 1 interacts with p53BP2, a protein which binds to the tumour suppressor p53. *FEBS Lett.* 377:295–300.

Hsieh-Wilson, L.C., P.B. Allen, T. Watanabe, A.C. Nairn, and P. Greengard. 1999. Characterization of the neuronal targeting protein spinophilin and its interactions with protein phosphatase-1. *Biochemistry.* 38:4365–4373.

Krasnoselsky, A.L., C.C. Whiteford, J.S. Wei, S. Bilke, F. Westermann, Q.R. Chen, and J. Khan. 2005. Altered expression of cell cycle genes distinguishes aggressive neuroblastoma. *Oncogene.* 24:1533–1541.

Kreivi, J.P., L. Trinkle-Mulcahy, C.E. Lyon, N.A. Morrice, P. Cohen, and A.I. Lamond. 1997. Purification and characterisation of p99, a nuclear modulator of protein phosphatase 1 activity. *FEBS Lett.* 420:57–62.

Lesage, B., M. Beullens, M. Nuytten, A. Van Eynde, S. Keppens, B. Himpens, and M. Bollen. 2004. Interactor-mediated nuclear translocation and retention of protein phosphatase-1. *J. Biol. Chem.* 279:55978–55984.

Mackeigan, J.P., L.O. Murphy, and J. Blenis. 2005. Sensitized RNAi screen of human kinases and phosphatases identifies new regulators of apoptosis and chemoresistance. *Nat. Cell Biol.* 7:591–600.

Moorhead, G., R.W. MacKintosh, N. Morrice, T. Gallagher, and C. MacKintosh. 1994. Purification of type 1 protein (serine/threonine) phosphatases by microcystin-Sepharose affinity chromatography. *FEBS Lett.* 356:46–50.

Ong, S.E., and M. Mann. 2005. Mass spectrometry-based proteomics turns quantitative. *Nat. Chem. Biol.* 1:252–262.

Tran, H.T., A. Ulke, N. Morrice, C.J. Johannes, and G.B. Moorhead. 2004. Proteomic characterization of protein phosphatase complexes of the mammalian nucleus. *Mol. Cell. Proteomics.* 3:257–265.

Trinkle-Mulcahy, L., P. Ajuh, A. Prescott, F. Claverie-Martin, S. Cohen, A.I. Lamond, and P. Cohen. 1999. Nuclear organisation of NIPP1, a regulatory subunit of protein phosphatase 1 that associates with pre-mRNA splicing factors. *J. Cell Sci.* 112:157–168.

Trinkle-Mulcahy, L., J.E. Sleeman, and A.I. Lamond. 2001. Dynamic targeting of protein phosphatase 1 within the nuclei of living mammalian cells. *J. Cell Sci.* 114:4219–4228.

Trinkle-Mulcahy, L., P.D. Andrews, S. Wickramasinghe, J. Sleeman, A. Prescott, Y.W. Lam, C. Lyon, J.R. Swedlow, and A.I. Lamond. 2003. Time-lapse imaging reveals dynamic relocalization of PP1gamma throughout the mammalian cell cycle. *Mol. Biol. Cell.* 14:107–117.

Van Eynde, A., S. Wera, M. Beullens, S. Torrekens, F. Van Leuven, W. Stalmans, and M. Bollen. 1995. Molecular cloning of NIPP-1, a nuclear inhibitor of protein phosphatase-1, reveals homology with polypeptides involved in RNA processing. *J. Biol. Chem.* 270:28068–28074.

Walker, M.G. 2001. Drug target discovery by gene expression analysis: cell cycle genes. *Curr. Cancer Drug Targets.* 1:73–83.

Wang, H., and D.L. Brautigan. 2002. A novel transmembrane Ser/Thr kinase complexes with protein phosphatase-1 and inhibitor-2. *J. Biol. Chem.* 277:49605–49612.

Zhao, S., and E.Y. Lee. 1997. A protein phosphatase-1-binding motif identified by the panning of a random peptide display library. *J. Biol. Chem.* 272:28368–28372.